BIOCHEMISTRY
including biophysical chemistry & molecular biology
Article

Biochemistry **2010,** *49,* 6093–6103 6093
DOI: 10.1021/bi100473v

Identification of the Structural Determinants for the Stability of Substrate and Aminoacrylate External Schiff Bases in *O*-Acetylserine Sulfhydrylase-A[†]

Hui Tian,[‖] Rong Guan,[‖] Enea Salsi,[‡] Barbara Campanini,[‡] Stefano Bettati,[‡,§] Vidya Prasanna Kumar,[‖] William E. Karsten,[‖] Andrea Mozzarelli,*[,‡,§] and Paul F. Cook*[,‖]

[‡]*Dipartimento di Biochimica e Biologia Molecolare, V. le G.P. Usberti 23/A, 43124 Parma, Italy,* [§]*Istituto Nazionale di Biostrutture e Biosistemi, Rome, Italy, and* [‖]*Department of Chemistry and Biochemistry, University of Oklahoma, 620 Parrington Oval, Norman, Oklahoma 73018*

Received March 30, 2010; Revised Manuscript Received June 14, 2010

ABSTRACT: *O*-Acetylserine sulfhydrylase is a pyridoxal 5′-phosphate (PLP)-dependent enzyme that catalyzes the final step in the cysteine biosynthetic pathway in enteric bacteria and plants, the replacement of the *β*-acetoxy group of *O*-acetyl-L-serine (OAS) by a thiol to give L-cysteine. Previous studies of the K41A mutant enzyme showed L-methionine bound in an external Schiff base (ESB) linkage to PLP as the enzyme was isolated. The mutant enzyme exists in a closed form, optimizing the orientation of the cofactor PLP and properly positioning active site functional groups for reaction. The trigger for closing the active site upon formation of the ESB is thought to be interaction of the substrate α-carboxylate with the substrate-binding loop comprised of T68, S69, G70, and N71, and Q142, which is positioned above the cofactor as one looks into the active site. To probe the contribution of these residues to the active site closing and orientation of PLP in the ESB, T68, S69, N71, and Q142 were changed to alanine. Absorbance, fluorescence, near UV−visible CD, and ^{31}P NMR spectral studies and pre-steady state kinetic studies were used to characterize the mutant enzymes. All of the mutations affect closure of the active site, but to differing extents. In addition, the site appears to be more hydrophilic given that the ESBs do not exhibit a significant amount of the enolimine tautomer. No buildup of the α-aminoacrylate intermediate (AA) is observed for the T68A and Q142A mutant enzymes. However, pyruvate is produced at a rate much greater than that of the wild-type enzyme. Data suggest that T68 and Q142 play a role in stabilizing the AA. Both residues donate a hydrogen bond to one of the carboxylate oxygens of the methionine ESB and may also be responsible for the proper orientation of the ESB to generate the AA. The S69A and N71A mutants exhibit formation of the AA, but the rate constant for its formation from the ESB is decreased by 1 order of magnitude compared to that of the wild type. S69 donates a hydrogen bond to the substrate carboxylate in the ESB, while N71 donates hydrogen bonds to O3′ of the cofactor and the carboxylate of the ESB; these side chains may also affect the orientation of the ESB. Data suggest that interaction of intermediates with the substrate-binding loop and Q142 gives a properly aligned Michaelis complex and facilitates the *β*-elimination reaction.

O-Acetylserine sulfhydrylase (OASS)[1] catalyzes a pyridoxal 5′-phosphate (PLP)-dependent replacement of the *β*-acetoxy group of *O*-acetyl-L-serine (OAS) with bisulfide to give L-cysteine (*1*). There are two isozymes of OASS, A and B, which are thought to be expressed under aerobic and anaerobic conditions, respectively (*2*). The A isozyme has been extensively studied with respect to its kinetic mechanism (*3*−*7*), chemical mechanism (*6*, *8*, *9*), structure (*10*−*13*), and dynamics (*10*, *11*, *13*−*16*), while the B isozyme has been studied to a lesser extent (*17*).

Briefly, the sulfhydrylase exhibits a ping-pong kinetic mechanism (*3*, *5*) with rate-limiting concerted *trans* α,*β*-elimination of the α-proton and the *β*-acetoxy group to generate the α-aminoacrylate intermediate (AA) (Scheme 1) (*8*). As the substrate external Schiff base (ESB) is formed prior to the α,*β*-elimination step, the active site closes and likely opens partially as the acetoxy group is eliminated (*15*, *16*). The second half-reaction, i.e., addition of bisulfide to give the cysteine ESB followed by its release, is very fast (*3*). Using analogues of bisulfide, the rate-limiting step is the final release of the cysteine product (*7*).

In spite of the substantial effort expended in the study of the mechanism of OASS-A, there are still a number of important questions that have not been answered. Closure of the active site is presumably triggered by the interaction of the α-carboxylate of OAS with the substrate-binding loop comprised of residues 68-TSGN-71 (Figure 1), and it has been proposed that this interaction

[†]This work was supported by the Grayce B. Kerr endowment to the University of Oklahoma to support the research of P.F.C. and grants from the Italian Ministry of University and Research (COFIN2007 to A.M.) and the International Exchange Program 2005 (to A.M. and P.F.C.).

*To whom correspondence should be addressed. A.M.: e-mail, andrea.mozzarelli@unipr.it; telephone, +39-0521-905138; fax, +39-0521-905151. P.F.C.: e-mail, pcook@ou.edu; telephone, (405) 325-4581; fax, (405) 325-7182.

[1]Abbreviations: AA, α-aminoacrylate external Schiff base; AAT, aspartate aminotransferase; CD, circular dichroism; Ches, 2-(*N*-cyclohexylamino)ethanesulfonic acid; ESB, external Schiff base; Hepes, *N*-(2-hydroxyethyl)piperazine-*N*′-2-ethanesulfonic acid; IPTG, isopropyl thio-*β*-D-galactoside; ISB, internal Schiff base; Mes, 2-(*N*-morpholino)ethanesulfonic acid; OAS, *O*-acetyl-L-serine; OASS-A, A isozyme of *O*-acetylserine sulfhydrylase; PLP, pyridoxal 5′-phosphate; RSSF, rapid scanning stopped flow; SAT, serine acetyltransferase; S-CNP-cysteine, *S*-(3-carboxy-4-nitrophenyl)-L-cysteine; SDS−PAGE, sodium dodecyl sulfate−polyacrylamide gel electrophoresis; TNB, 5-thio-2-nitrobenzoate; TS, tryptophan synthase; WT wild type.

Published on Web 06/15/2010

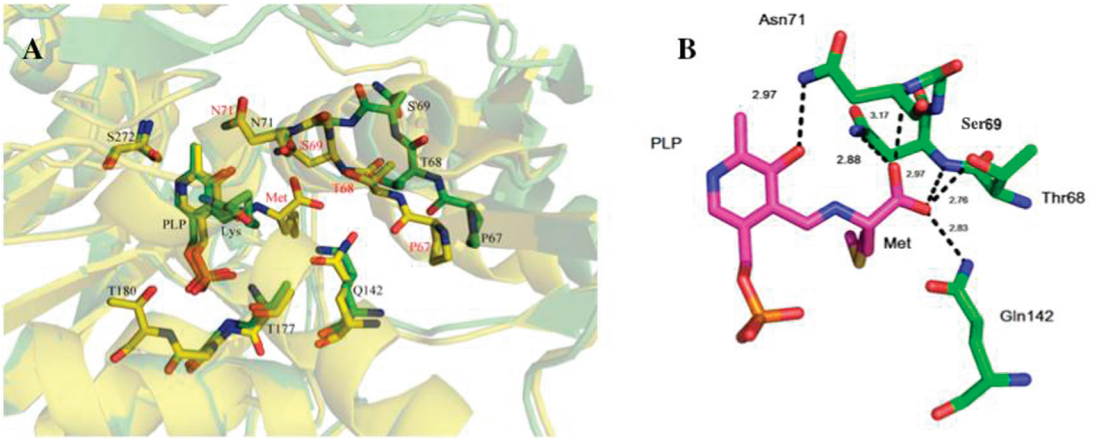

FIGURE 1: Active site structures of OASS-A. (A) Overlay of the active sites of the wild-type free enzyme (green) and the methionine ESB of the K41A mutant enzyme (yellow) (*9*). L-Methionine induces a conformational change in the substrate-binding loop that results in closure of the active site. Note the change in the position of S69. (B) Close-up view of the active site of OASS-A featuring the interaction among the methionine ESB, the substrate-binding loop, and Q142. The phenolic oxygen of PLP is within hydrogen bonding distance of N71. Q142, S69, and T68 donate hydrogen bonds to O^1 of the methionine carboxylate. S69 and N71 donate hydrogen bonds to O^2 of methionine carboxylate. Figures were generated via PyMol using Protein Data Bank entries 1OAS and 1D6S for panel A and 1OAS for panel B.

Scheme 1: Minimal Chemical Mechanism of OASS-A[a]

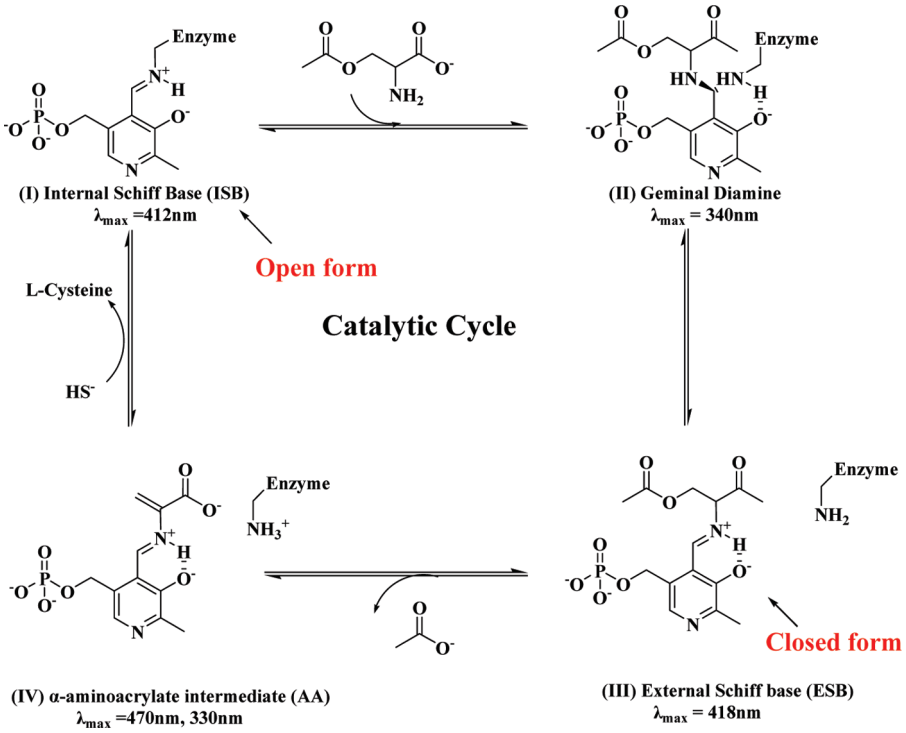

[a]The reaction begins with binding of OAS to the ISB (I) and proceeds to the AA (IV) via *gem*-diamine (II) and ESB (III) intermediates.

stabilizes the OAS ESB and helps to position it for the subsequent elimination reaction. In addition, Q142 is positioned above the planar ESB and donates a hydrogen bond to the substrate α-carboxylate group of ESB and AA, thus aiding in stabilizing both intermediates. In tryptophan synthase, an enzyme belonging to the same fold type II of OASS, mutations of amino acids interacting with the substrate or forming a salt bridge were seen to strongly influence reactivity and to stabilize alternative conformations of the β-subunit (*27*−*29*).

In this work, we have prepared mutant enzymes with changes in residues of the substrate-binding loop and at position Q142. The mutant enzymes have undergone an in-depth characterization using UV−visible, fluorescence, near UV−visible CD, and ^{31}P NMR spectral measurements, as well as pre-steady state kinetic studies of the first half-reaction. Data suggest T68 and Q142 play a role in stabilizing the AA intermediate, while S69 and N71 are mainly involved in stabilizing and orienting the ESB.

MATERIALS AND METHODS

Chemicals. The buffers Hepes, Mes, and Ches were from Research Organics. L-Cysteine, L-serine, OAS, NADH, and lactate dehydrogenase were obtained from Sigma. All restriction enzymes and T4 DNA ligase were from Promega. The DNA sequencing kit and restriction enzymes were purchased from Promega or USB. For plasmid purification, the Nucleobond AX kit (The Next Group, Inc.) was used. The substrate, TNB, was

prepared by reduction of DTNB (Aldrich) just prior to use (*3*). All other chemicals and reagents were obtained from commercial sources and were of the highest purity available.

Expression and Purification of OASS-A. The *cysK* gene encoding *St*OASS-A was subcloned into a pET16b vector via *Nde*I and *Xho*I sites, using a pCKM3 vector provided by N. M. Kredich (*25*). The following forward and reverse primers were used for the polymerase chain reaction (PCR) of the *cysK* gene: *St*OASS-A_f (GGAATTC**CATATG**AGTAAGATTTATGAA-GATAACTCGC) and *St*OASS-A_r (CCG**CTCGAG**TCACTG-TTGCAGTTCTTTCTC). PCR conditions were as follows: (1) 95 °C for 1 min, (2) 95 °C for 30 s, (3) 50 °C for 1 min, and (4) 68 °C for 2 min and 30 s. This was followed by thirty cycles of steps 2−4, followed by step 5 (68 °C for 10 min). The pET16b vector and the amplified DNA fragment were digested with *Nde*I and *Xho*I, respectively, and then ligated to obtain the new construct. This new construct encoded an N-terminal 10-His-tagged enzyme and was transformed into *Escherichia coli* BL21-(DE3)-RIL cells for expression (*26*). An induction culture was grown at 30 °C in LB medium containing ampicillin (100 μg/mL). When the induction culture reached an OD_{600} of 0.7−0.9, it was induced by the addition of 0.5 mM IPTG and allowed to grow for 5 h. The pH was maintained at 7.0 during growth using 10 N KOH and 2 N HCl. After centrifugation at 8000*g* for 30 min, the cell pellet was resuspended in sonication buffer that contains 50 mM phosphate (pH 7.8) and 300 mM NaCl. The cells were sonicated for 3 min with a 30 s rest time between each minute of pulse. PLP (0.05 g) was added to the supernatant, which was stirred for 1 h at 4 °C. The supernatant was loaded onto a Ni-NTA agarose affinity column (15 mL bed volume), which was pre-equilibrated with sonication buffer, and the column was washed with 10 bed volumes of 50 mM imidazole in sonication buffer. The column was then developed in steps of 50 mM imidazole using 10 bed volumes, and OASS-A eluted between 0.15 and 0.2 M imidazole. The enzyme was dialyzed against 4 L of 10 mM Hepes (pH 8.0), concentrated to 10 mg/mL, and stored at −80 °C. SDS−PAGE showed the enzyme to be more than 98% pure.

Preparation of the Mutant Enzymes. Mutant plasmids in which T68, S69, N71, and Q142 were individually replaced with alanine were prepared using QuikChange mutagenesis via PCR according to previously published procedures (*26*). The following primers were used for these mutant enzymes (mutated codon in bold): T68A, 5′-GTG GAG CCG **GCC** AGC GGC AAC ACC GGT ATT G-3′ (forward primer) and 5′-C AAT ACC GGT GTT GCC GCT **GGC** CGG CTC CAC-3′ (reverse primer); S69A, 5′-AA CTG GTGGG CCG ACC **GCC** GGC AAC ACC GGT ATT-3′ (forward primer) and 5′-AAT ACC GGT GTT GCC **GGC** GGT CGG CTC CAC CAG TT-3′ (reverse primer); N71A, 5′-CG ACC AGC GGC **GCC** ACC GGT ATT GC-3′ (forward primer) and 5′-GC AAT ACC GGT **GGC** GCC GCT GGT CG-3′ (reverse primer); Q142A, 5′-CAA AAA TAT CTC CTG CTC CAG **GCG** TTC AGC AAC C-3′ (forward primer) and 5′-G GTT GCT GAA **CGC** CTG GAG CAG GAG ATA TTT TTG-3′ (reverse primer).

The resulting mutant genes were completely sequenced to be sure no other mutations were present, and none were found. Mutant proteins were then isolated using the same method that was used for the wild-type (WT) plasmid-containing strain (*9*). The cell mass from overnight growths and the amount of mutant proteins obtained were similar to those obtained for WT.

UV−Visible Spectral Studies. UV−visible spectra were recorded on a Hewlett-Packard, model 8453, photodiode array spectrophotometer. Spectra of the T68A, S69A, N71A, and Q142A mutant enzymes were recorded at pH 6.5 in 100 mM Hepes in the absence and presence of 1 mM OAS and at pH 9.5 in 100 mM Ches in the absence and presence of 10 mM L-cysteine or 100 mM L-serine. Spectra were recorded from 300 to 550 nm using 1 cm path length cuvettes at 25 °C. Buffer and amino acid blanks were subtracted from the sample spectra. Enzyme concentrations varied throughout these studies, and data are therefore presented relative to the ISB.

Fluorescence Studies. Fluorescence spectra of WT and mutant enzymes were recorded on a Shimadzu RF-5301 PC spectrofluorometer in the absence and presence of amino acids at 25 °C. Spectra of T68A, S69A, N71A, and Q142A mutant enzymes were measured at pH 6.5 in 100 mM Hepes in the absence and presence of 1 mM OAS and at pH 9.5 in 100 mM Ches in the absence and presence of 10 mM L-cysteine or 100 mM L-serine. Excitation was at 298 nm, and the excitation and emission slits were set to 5 nm. Emission was measured over the wavelength range from 310 to 580 nm. Buffer and amino acid blanks were subtracted from the sample spectra. Enzyme concentrations varied throughout these studies, and data are therefore presented as the ratio of fluorescence emission of tryptophan to that at long wavelengths.

Circular Dichroism Studies. CD spectra were recorded on an Aviv 62 DS spectropolarimeter at 25 °C with a path length of 0.2 cm. Enzyme concentrations of 2.9 and 116 μM were used for far UV and near UV−visible spectra, respectively. The buffer used for far UV CD spectra was 100 mM Hepes (pH 7.0) for near UV−visible spectra of the ISB and AA and 100 mM Ches (pH 9.0) for near UV−visible spectra in the presence of serine and cysteine. A buffer blank was subtracted from each spectrum. Spectra were collected with a dwell time of 2 s, and three spectra were averaged. Far-UV spectra were measured from 200 to 250 nm, while near UV−visible spectra were measured from 300 to 550 nm.

^{31}P NMR Spectroscopy. Fourier transform ^{31}P NMR spectra were recorded at 161.909 MHz on a Varian VNMRS 400 SMB superconducting spectrometer using an autotunable dual broadband 5 mm probe head with broadband ^{1}H decoupling. The NMR tube, spinning at 15−20 Hz, contained the sample (0.6 mL) and D_2O (0.06 mL) as the field/frequency lock and was maintained at 20 ± 0.1 °C using a thermostated continuous air flow. A spectral width of 10000 Hz was acquired in 32K data points with a pulse angle of 60°. The exponential line broadening used prior to Fourier transformation was 10 Hz. Protein samples were dissolved in 100 mM Hepes or Ches buffer at the appropriate pH. Positive chemical shifts in parts per million are downfield changes with respect to 85% H_3PO_4.

Rapid Scanning Stopped Flow. Pre-steady state kinetic measurements were taken using an OLIS RSM 1000 stopped flow spectrophotometer in the multiple-wavelength mode. Sample solutions in 100 mM Mes (pH 6.5) were prepared in two syringes. The first syringe contained enzyme at a final concentration no lower than 2 μM, while the second syringe contained OAS at twice the final desired concentration. Experiments were repeated at several different concentrations of OAS (0.1−40 mM). Data were collected with a repetitive scan rate of 15 ms for S69 and N71 over the wavelength range of 300−600 nm, and the number of scans collected depended on the rate of the reaction. The appearance of the AA was monitored at 470 nm, and the

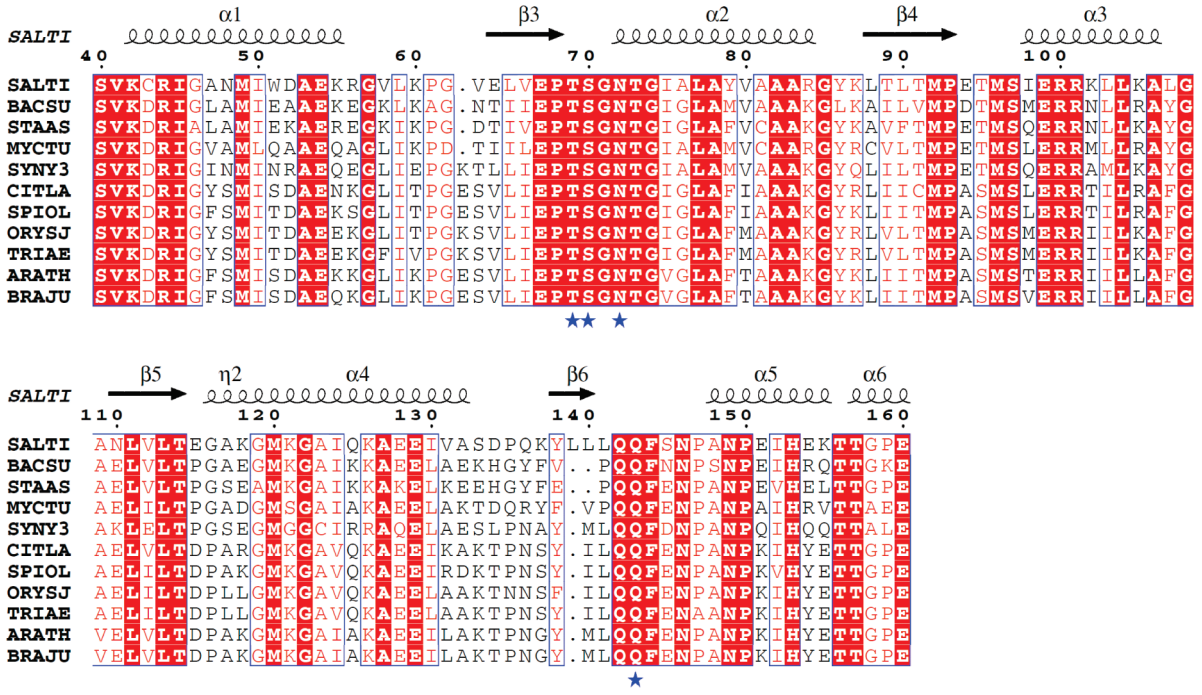

FIGURE 2: Multiple-sequence alignment of OASS-A. Sequences of OASS-A from bacteria and plants were retrieved from the ExPASy enzyme database (NiceZyme View). Plant sequences were from the cytoplasmic isoforms. Abbreviations: SALTY, *Salmonella typhimurium*; BACSU, *Bacillus subtilis*; STAAS, *Staphylococcus aureus*; MYCTU, *Mycobacterium tuberculosis*; SYNY3, *Synechocystis* sp. (strain PCC 6803); CITLA, *Citrullus lanatus*; SPIOL, *Spinacia oleracea*; ORYSJ, *Oryza sativa* subsp. Japonica; TRIAE, *Triticum aestivum*; ARATH, *Arabidopsis thaliana*; BRAJU, *Brassica juncea*. Sequence alignments were conducted using Vector NTI (Invitrogen), and the sequence conservation pattern was visualized using ESPript version 2.2 (*35*). A portion of the whole sequence is shown, i.e., from residue 40 to residue 160. Residues T68, S69, N71, and Q142 are marked with blue stars at the bottom of alignment. Secondary structure elements indicated above the alignment are from the *Salmonella* three-dimensional structure (Protein Data Bank entry 1OAS).

disappearance of the ISB was monitored at 412 nm. The reaction temperature was maintained at 25 °C using a circulating water bath.

Spectrophotometric Detection of Pyruvate in the First OASS Half-Reaction. The production of pyruvate in the first half of the OASS reaction was detected by coupling to the oxidation of NADH by lactate dehydrogenase. The initial rate of formation of pyruvate was measured by monitoring the oxidation of NADH at 340 nm with the OAS concentration fixed at 10 mM. The final concentration of NADH was fixed at 0.2 mM in a 0.5 mL reaction mixture, while the lactate dehydrogenase concentration was 10 units/mL. Experiments were conducted in 100 mM Mes (pH 6.5) at 25 °C. The concentrations of WT, T68A, and Q142A OASS were 15, 3, and 0.033 μM, respectively.

Data Processing. Rapid scanning stopped flow (RSSF) data were fitted using the software provided by OLIS. To obtain the first-order rate constant (k_{obs}) for the appearance of the AA, eq 1 was used.

$$A_t = A_0 e^{-k_{obs}t} \pm B_0 \quad (1)$$

where A_t is the absorbance at time t, A_0 is the absorbance at time zero, and B_0 corrects for the background absorbance.

All time courses (not shown) were collected under pseudo-first-order conditions. The dependence of k_{obs} on the concentration of OAS was fitted to eq 2.

$$k_{obs} = \frac{k_{max}\mathrm{OAS}}{K_{ESB} + \mathrm{OAS}} \quad (2)$$

where k_{max} is the value of k_{obs} at a saturating OAS concentration, which represents the rate constant for elimination of acetate from the OAS ESB, K_{ESB} is the constant for dissociation of OAS from the OAS ESB, and OAS is the concentration of OAS.

RESULTS

Binding of the substrate, OAS, to OASS-A and its subsequent conversion to the ESB result in the closure of the active site (*9*, *11*). The trigger proposed for active site closure is interaction of the substrate α-carboxylate with the substrate-binding loop, comprised of residues 68-TSGN-71 (*11*). Proposed strong hydrogen bonds are donated by T68, S69, and N71 (*15*). In addition, Q142 also donates a hydrogen bond to the α-carboxylate of the substrate in the ESB. The hydrogen bonding interactions between the enzyme and the α-carboxylate of the ESB likely serve to properly position and stabilize the ESB, and the AA intermediate, once the elimination of the β-acetoxy group of OAS has taken place. The residues of the substrate-binding loop and Q142 are highly conserved, suggesting their importance in the mechanism of OASS-A (Figure 2). To test the role of the residues in the substrate-binding loop and Q142, site-directed mutagenesis was used to change each of them in turn to alanine to eliminate their hydrogen bonding interaction.

UV−Visible Spectroscopy. The UV−visible spectrum of WT OASS-A exhibits an absorbance maximum at 412 nm reflecting the ketoenamine tautomer of the internal Schiff base (ISB) with a minor band at ~330 nm reflecting the enolimine tautomer (Scheme 2 and Figure 3) (*15*, *18*). Addition of OAS to the enzyme results in a shift in the λ_{max} from 412 to 470 nm with a concomitant increase in the absorbance at 330 nm as a consequence of formation of the α-aminoacrylate ESB (AA). The external Schiff base of serine shows a significant decrease in the absorbance at 412 nm, a shift in the maximum of the remaining

Scheme 2: Representation of the Ketoenamine to Enolimine Tautomerization that Occurs in the ISB, OAS ESB, L-Serine ESB, L-Lanthionine ESB, and AA Intermediates. The OAS ESB Is Used To Demonstrate the Equilibria; Experimentally Determined λ_{max} Values Are Provided (*15*, *18*)

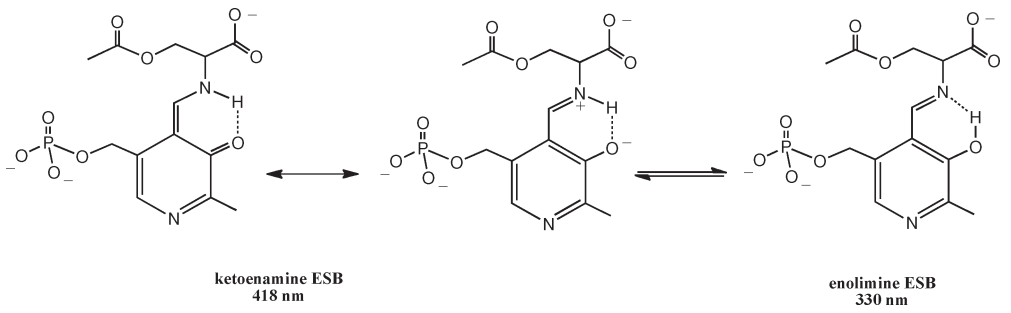

Table 1: UV−Visible Extinction Coefficients Relative to the ISB

	WT[a]	S69A	N71A	T68A	Q142A
ISB	$\varepsilon^{rel}_{412} = 1.0$	$\varepsilon^{rel}_{412} = 1.0$	$\varepsilon^{rel}_{412} = 1.0$	$\varepsilon^{rel}_{412} = 1.0$	$\varepsilon^{rel}_{412} = 1.0$
AA	$\varepsilon^{rel}_{470} = 1.28$ $\varepsilon^{rel}_{330} = 0.82$	$\varepsilon^{rel}_{470} = 1.05$ $\varepsilon^{rel}_{330} = 1.045$	$\varepsilon^{rel}_{470} = 1.22$ $\varepsilon^{rel}_{330} = 1.16$	not applicable	not applicable
ESB_{serine}	$\varepsilon^{rel}_{418} = 0.53$ $\varepsilon^{rel}_{330} = 0.53$	$\varepsilon^{rel}_{412} = 1.32$ $\varepsilon^{rel}_{330} = 0.72$	$\varepsilon^{rel}_{420} = 1.21$ $\varepsilon^{rel}_{330} = 0.75$	$\varepsilon^{rel}_{414} = 0.98$	$\varepsilon^{rel}_{414} = 0.99$
$ESB_{lanthionine}$	$\varepsilon^{rel}_{418} = 1.03$	$\varepsilon^{rel}_{412} = 1.02$	$\varepsilon^{rel}_{424} = 1.22$	$\varepsilon^{rel}_{414} = 0.99$	$\varepsilon^{rel}_{414} = 1.0$

[a]Values are relative to the ISB for the respective mutant enzyme. Extinction coefficients were as follows for WT: ISB, $\varepsilon_{412} = 7600\ M^{-1}\ cm^{-1}$; AA, $\varepsilon_{470} = 9760\ M^{-1}\ cm^{-1}$ and $\varepsilon_{330} = 6250\ M^{-1}\ cm^{-1}$; Ser ESB, $\varepsilon_{418} = 4000\ M^{-1}\ cm^{-1}$ and $\varepsilon_{330} = 4000\ M^{-1}\ cm^{-1}$; lanthionine ESB, $\varepsilon_{418} = 7840\ M^{-1}\ cm^{-1}$.

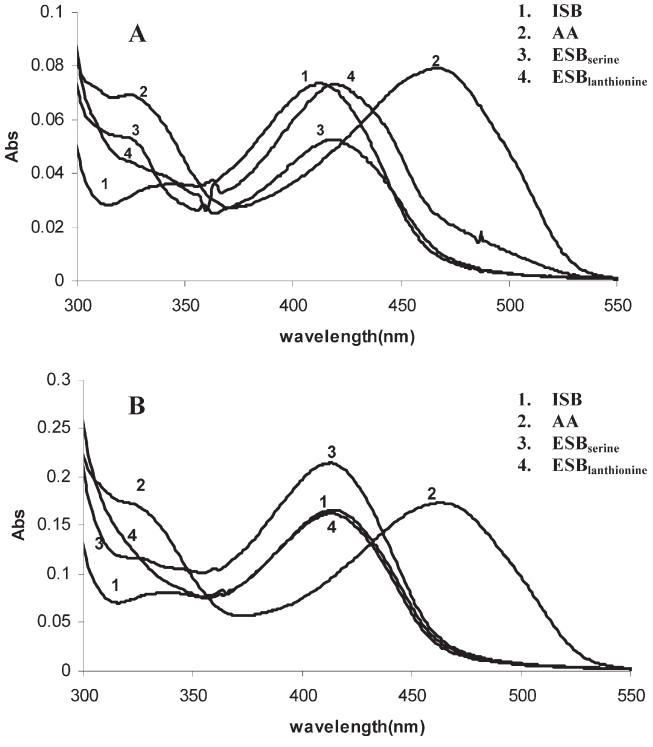

FIGURE 3: UV−visible absorbance spectra of WT OASS-A (A) and S69A (B). Absorbance spectra in the absence and presence of amino acids were recorded at 25 °C. Spectra of the ISB and AA (1 mM OAS) were recorded in 100 mM Hepes (pH 6.5), while spectra in the presence of 100 mM L-serine and 10 mM L-cysteine were recorded in 100 mM Ches (pH 9.5).

absorbance to 418 nm, and an increase in the absorbance at 330 nm (*15*). The lanthionine ESB,[2] formed upon addition of cysteine, gives a shift in the λ_{max} from 412 to 418 nm and an increase in the absorbance at 330 nm resulting from the free cysteine in solution at pH 9.5.[3]

Spectra were recorded in an identical manner for each of the four mutant enzymes, T68A, S69A, N71A, and Q142A. Spectra for the S69A mutant enzyme are shown in Figure 3 (spectra for the remaining mutant enzymes have been deposited as Supporting Information, Figure S1). The ISB and AA spectra are qualitatively identical to those of WT, indicating the enzyme is capable of catalyzing the first half-reaction. However, formation of the serine ESB results in a 30% increase in the extinction coefficient at 412 nm (with no appreciable red shift of the ketoenamine maximum absorbance) and a less pronounced increase in the 330 nm absorbance. Formation of the lanthionine ESB upon addition of cysteine[2] gives only an increase in the absorbance at 330 nm, resulting from the thiolate of cysteine.[3] Similar results are observed for the N71A mutant enzyme. The ISB exhibits a maximum at 412 nm, while the AA is formed, and again gives nearly equal extinction coefficients at λ_{470} and λ_{330}. A significant red shift in the serine and lanthionine ESBs is consistent with a more hydrophilic environment in the N71A mutant enzyme. In both cases, the ketoenamine tautomer is favored, compared to the serine ESB of WT, in agreement with a more hydrophilic site, perhaps because it is more open.

The UV−visible spectra of the T68A and Q142A mutant enzymes are similar. There is no evidence of the AA for either mutant enzyme, suggesting it is not formed or very unstable. Addition of L-serine or L-cysteine to the mutant enzymes gives an only slight shift in the maximum absorbance to 414 nm for both mutant enzymes. The ketoenamine tautomer (414 nm) of these mutant enzymes dominates, suggesting a polar environment. The λ_{max} values and extinction coefficients relative to those of the ISB are listed in Table 1.

[2]Addition of cysteine to OASS results in a rapid, transient formation of the AA followed by attack by a second cysteine thiol to generate the lanthionine ESB (*6*, *21*).

[3]The observed increase in absorbance below 330 nm in the presence of 10 mM L-cysteine at pH 9.5 is a result of the thiolate of cysteine (the thiol has a pK_a of 8.7). Ionization of the L-cysteine thiol gives an increase in absorbance centered at 235−240 nm ($\varepsilon = 4500\ M^{-1}\ cm^{-1}$) (*34*).

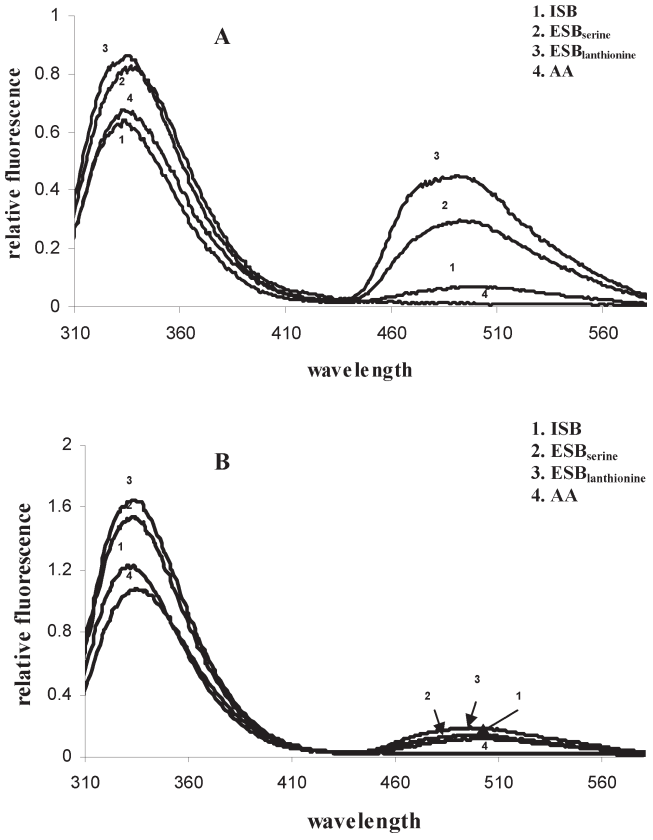

FIGURE 4: Fluorescence emission spectra of WT OASS-A (A) and S69A (B). Fluorescence spectra in the absence and presence of amino acids were recorded at 25 °C. Spectra for the ISB and AA were recorded in 100 mM Hepes (pH 6.5), while spectra for the serine and lanthionine ESBs were recorded in 100 mM Ches (pH 9.5). Excitation was at 298 nm, and spectra were corrected for those of buffer and amino acids alone.

From the data given above, S69 and N71 appear to play a role in properly orienting the ESB, while T68 and Q142 likely play an important role in stabilizing the AA intermediate. Consistent with this, a higher percentage of the ketoenamine tautomer suggests a more hydrophilic environment in the active sites of these mutant enzymes, likely due to a more open active site.

Fluorescence Spectroscopy. OASS-A has two tryptophan residues, W50 in the N-terminal domain and W161 in the C-terminal domain. Fluorescence emission spectra (excitation at 298 nm) exhibit two maxima, one at 337 nm and a broad band from 492 to 500 nm (Figure 4). The 337 nm emission is a result of intrinsic tryptophan fluorescence. The long wavelength band results from singlet to singlet energy transfer from tryptophans (mainly W50) to the cofactor enolimine that, in the excited state, undergoes an interconversion to ketoenamine that emits at ~500 nm (*14*, *16*, *19*, *22*, *23*). Formation of the serine or lanthionine ESB results in an enhancement of the long wavelength fluorescence band of WT with a decrease in the ratio of fluorescence intensities at 337 and 500 nm, as a result of a change in the distance and/or orientation of PLP compared to that of tryptophans, which facilitates the energy transfer. As the ESB is formed, PLP tilts 13° such that C4′ approaches the active site entrance (*11*). In addition, the emission maximum is blue-shifted from 500 to 492 nm, suggesting a more hydrophobic environment around the ESB intermediate, due to the closure of the active site induced by ligand binding. A significant quenching of the long wavelength fluorescence emission maximum is observed in the presence of OAS, concomitant with formation of the AA intermediate. The probable reason is attributed to a decrease in the efficiency of Förster resonance energy transfer.

Table 2: Ratios of Intrinsic Tryptophan to Long Wavelength Fluorescence

	WT[a]	T68A	S69A	N71A	Q142A
ISB	9.2	11.1	8.6	7.9	19.6
ESB$_{serine}$	2.8	14.4	12.5	2.7	9.8
ESB$_{lanthionine}$	1.9	13.1	8.6	3.4	3.0

[a]Ratio of intrinsic fluorescence at 337 nm to long wavelength fluorescence around 500 nm. The maximum for long wavelength fluorescence depends on the enzyme form and mutation. The maximum for the ISB is 500 nm in all cases. The maximum for the ESBs is 492 nm for WT and Q142A and 500 nm for all other mutant enzymes.

Fluorescence emission spectra obtained for the S69A mutant enzyme also exhibit two maxima, 337 and 500 nm (Figure 4) (spectra for the remaining mutant enzymes have been deposited as Supporting Information, Figure S2). The ratio of fluorescence intensities at 337 and 500 nm for the ESB is 8.6, similar to the value of 9.2 observed for WT (Table 2). The F_{337}/F_{500} ratio exhibits no decrease in the presence of serine and cysteine, suggesting that either the repositioning of the cofactor compared to tryptophan in enzyme does not occur or the lifetime of the excited species is much shorter, since the active site is probably more open in the mutant enzyme. However, formation of the AA is observed as shown by the loss of long wavelength fluorescence, consistent with the UV−visible spectra (Figure 3).

Spectra for the T68A mutant enzyme differ significantly from those of WT (Figure S2 of the Supporting Information). The 337 and 500 nm peaks are observed, but long wavelength fluorescence is reduced compared to that of WT (Table 2). In addition, the fluorescence of the ESBs results in almost no change at 500 nm, with no increase in the level of energy transfer.

On the other hand, spectra obtained for the N71A mutant enzyme are similar to those of the WT (Figure S2). Formation of the serine and cysteine ESBs results in an increase in the long wavelength fluorescence such that F_{337}/F_{500} is more similar to that of WT. Formation of the AA results in a band at 550 nm, which results from emission of the ketoenamine formed from the enolimine by proton transfer in the excited state (*16*).

The spectrum of the Q142A mutant enzyme exhibits maxima at 337 and 492 nm (Figure S2) and a fluorescence ratio of 19.6 compared with a ratio of 9.2 for WT (Table 2). Addition of 100 mM L-serine or 10 mM L-cysteine results in a significant enhancement in long wavelength emission at 500 nm, and a blue shift similar to that of WT, but the amplitude of this long wavelength enhancement is smaller than that of WT. Addition of 1 mM OAS gives no loss of the long wavelength fluorescence, indicating the AA does not form or is unstable. Fluorescence data are consistent with the UV−visible absorbance spectra and suggest an important role for Q142 in stabilization of the AA intermediate.

Consistent with the absorbance spectra, fluorescence data indicate that there is no buildup of the AA intermediate in the T68A and Q142A mutant enzymes, consistent with these residues stabilizing the AA. N71 and S69 appear to be involved in orientation of the cofactor PLP, with S69 being the more important of the two.

Circular Dichroism. Chiral molecules exhibit a CD spectrum as a result of absorbing left- and right-handed polarized light to different extents. Proteins are composed of optically active

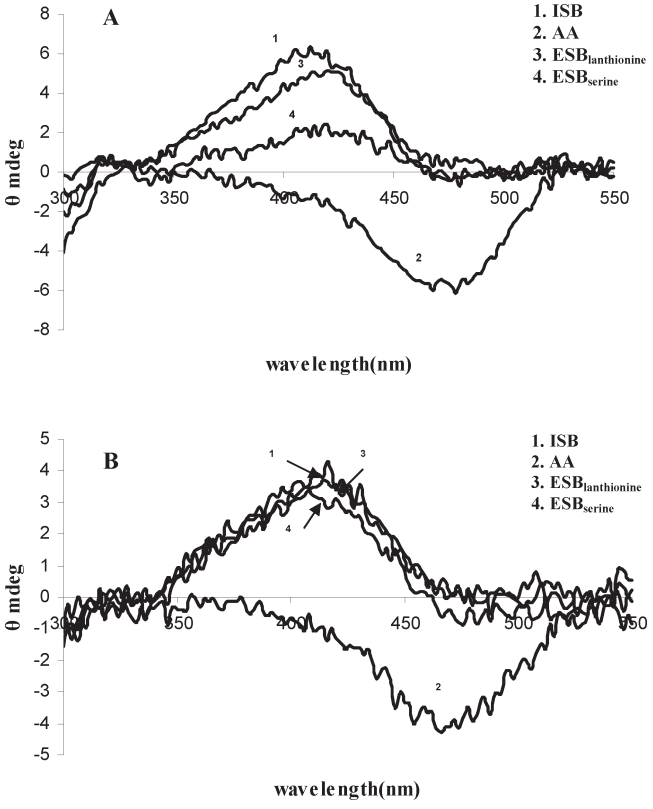

FIGURE 5: Near UV−visible circular dichroic spectra of WT OASS-A (A) and S69A (B). Spectra were recorded with 116 μM enzyme, in 100 mM Hepes (pH 7.0) for the ISB and AA, while those for the ESBs were recorded in 100 mM Ches (pH 9.0).

elements and can adopt different types of three-dimensional structures; each type of molecule produces its own CD spectrum. The wavelengths of light that are most useful for examining the secondary structures of enzymes are in the far-UV ranges (from 190 to 300 nm). Near UV−visible CD spectra (from 300 to 550 nm) are useful as a probe of the asymmetric interaction of the small molecules (ligand) with the protein matrix, called induced CD. Changes in the near UV−visible CD spectrum may reflect changes in the interaction of the protein matrix with a small molecule. Even though many ligands may be intrinsically achiral, their unique orientation on binding to a protein, coupled to their specific asymmetric interaction with the protein, can cause them to acquire CD properties (*24*). The far UV CD spectra of all of the mutant enzymes are identical to those of WT (data not shown).

The near UV−visible CD spectrum of the ISB of OASS-A gives an induced CD signal centered at 412 nm (Figure 5), as in the absorbance spectrum (Figure 3). The signal changes significantly when substrates are added. Addition of L-cysteine or L-serine induces a shift in λ_{max} from 412 to 418 nm, as also observed in visible absorbance spectra. The positive Cotton effect of the ISB and the ESBs is consistent with asymmetric binding of the ketoenamine tautomer of the cofactor. A smaller signal is also seen for the enolimine tautomer centered at 330 nm with a negative Cotton effect. The AA formed by adding OAS is centered at 330 and 470 nm as expected, but both tautomers exhibit a negative Cotton effect. The negative Cotton effect reflects a difference in the chromophore, likely in the magnetic dipole moment of the AA intermediate compared to the ISB and ESB. The ellipticity of the positive Cotton effect of the ISB and the negative Cotton effect of the AA is identical (Table 3).

Table 3: Ellipticity from CD Spectra for WT and Mutant Enzymes

	WT	T68A	S69A	N71A	Q142A
ISB	θ_{412}, 6.3	θ_{412}, 1.4	θ_{412}, 3.9	θ_{412}, 4.9	θ_{412}, 1.3
ESB$_{serine}$	θ_{418}, 2.4	θ_{414}, 3.2	θ_{412}, 3.1	θ_{421}, 5.4	θ_{416}, 3.9
ESB$_{lanthionine}$	θ_{418}, 4.9	θ_{414}, 1.9	θ_{412}, 3.5	θ_{424}, 9.8	θ_{416}, 2.6
AA	θ_{470}, −5.6	not applicable	θ_{470}, −4.1	θ_{470}, −4.9	not applicable

Table 4: Summary of ^{31}P NMR Data of the WT and Mutant Enzymes[a]

	WT	T68A	S69A	N71A	Q142A
ISB	δ = 5.20	δ = 5.19	δ = 5.22	δ = 5.19	δ = 5.22
	lw = 20.5	lw = 20.1	lw = 21.0	lw = 21.3	lw = 20.8
ESB$_{serine}$	δ = 4.40	δ = 5.18	δ = 5.21	δ = 5.36	δ = 5.21
	lw = 50.7	lw = 17.4	lw = 30.2	lw = 40.0	lw = 29.6
ESB$_{lanthionine}$	δ = 5.40	δ = 5.14	δ = 5.23	δ = 5.10	δ = 5.26
	lw = 35.7	lw = 17.3	lw = 24.9	lw = 28.9	lw = 26.8

[a] ^{31}P NMR spectra were recorded in 100 mM Ches (pH 9) as discussed in Materials and Methods. λ is the chemical shift in parts per million, while lw is the line width in hertz.

The S69A and N71A mutant enzymes exhibit CD spectra that are qualitatively similar to those of WT (Figures 5 and Figure S3 of the Supporting Information). The ellipticities of the ISB and AA are equal, but lower than those of WT, and the S69A mutant enzyme exhibits the lower of the two. The serine ESB has a higher ellipticity for the mutant enzymes compared to WT, while that of the lanthionine ESB has a slightly lower ellipticity for S69A but is twice that of WT for N71A (Table 3).

Spectra of the T68A and Q142A mutant enzyme are similar to one another but differ considerably compared to those of WT (Figure S3). Either no AA intermediate is formed, or it is unstable as judged by the absence of the negative Cotton effect in the presence of OAS, in agreement with visible absorbance and fluorescence spectra. The ellipticities of the ISB and serine and lanthionine ESBs exhibit lower ellipticities compared to the WT ellipticity.

The near UV−visible CD spectra corroborate the UV−visible absorbance spectral data. The induced Cotton effect reflects the asymmetric interaction of the cofactor with the protein matrix. The change in ellipticity for the T68A, S69A, and Q142 mutant enzymes suggests they have a higher cofactor mobility than the WT, while the N71A mutant enzyme exhibits a higher ellipticity for the ESB intermediates, suggesting a stronger asymmetric interaction between the cofactor PLP and the protein matrix.

^{31}P NMR. ^{31}P NMR provides a powerful tool that allows one to obtain direct evidence on the environment around the 5′-phosphate of PLP bound to enzymes (*15*, *18*). The chemical shift reflects the protonation state of the 5′-phosphate and the tightness of its binding to the protein. The line width provides information about the freedom of rotation of the 5′-phosphate group. The two parameters can be used to describe conformational changes that occur along the reaction pathway of OASS-A. The chemical shift of the WT ISB is 5.2 ppm (Table 4), indicative of a dianionic 5′-phosphate that is very tightly bound to the active site (*15*). A line width of 21 Hz is observed for the phosphate resonance, indicative of a 5′-phosphate that tumbles with the protein as expected for a tightly bound phosphate. Addition of 15 mM L-cysteine to the WT enzyme induced a slight downfield shift to 5.3 ppm, suggesting an even tighter binding of the 5′-phosphate, likely as a result of the long lanthionine side chain

Table 5: Pre-Steady State Kinetic Parameters[a]

	WT	S69A	N71A
K_{ESB} (mM)	0.54 ± 0.18	0.13 ± 0.03 (−4)	6 ± 2 (11)
k_{max} (s^{-1})	13.6 ± 3.9	1.6 ± 0.4 (−9)	0.60 ± 0.15 (−23)

[a]Final enzyme concentrations were ≥2 μM. All experiments were conducted in 100 mM Hepes (pH 7) at 25 °C. k_{max} is the rate constant for formation of the AA from the OAS ESB.

that is more tightly bound.[2] A broad line width suggests two species in equilibrium. It should be noted that if two species interconvert slowly, two distinct resonances are observed. If the equilibration is rapid, a single sharp resonance is observed. If the equilibration exhibits an intermediate rate, a broad peak is obtained at the average of the two resonances, weighted toward the dominant species of the two. The line width of the OASS-A with L-cysteine is 35.7 Hz, which suggests that two species, the enolimine and ketoenamine tautomers, are exchanging. With 100 mM L-serine, the chemical shift of 4.4 ppm suggests a significant loosening of the binding of the cofactor at the 5′-phosphate. In addition, a line width of 50 Hz indicates an apparent equilibrium between ketoenamine and enolimine tautomers, consistent with the UV−visible spectral data.

The ISB of all of the mutant enzymes exhibits a chemical shift very similar to that of WT. In the presence of L-cysteine or L-serine, the chemical shifts remain about the same, and the line widths become narrow compared to those of WT. Data suggest no change in the tightness of binding of the 5′-phosphate. The broader line width in the presence of serine suggests species interconversion as for WT, but the rate of exchange between the ketoenamine and enolimine tautomer must increase to account for the narrower line width compared to that of WT.

Pre-Steady State Kinetic Studies. Rapid scanning stopped flow experiments, mixing the S69A or N71A mutant enzymes with OAS, gave spectra that show a decrease in the absorbance at 412 nm and an increase in the absorbance at 330 and 470 nm, consistent with the formation of the AA. Spectra exhibit a single isosbestic point at 430 nm, indicative of the interconversion of the ISB and AA with no other intermediates present at a significant concentration (data not shown). A fit of the observed first-order rate constant (obtained by monitoring the change in absorbance at 470 nm) versus OAS concentration to eq 2 gave values of K_{ESB} and k_{max} of 0.13 mM and 1.6 s^{-1}, respectively, for S69A and values of 6.0 mM and 0.6 s^{-1}, respectively, for N71A. Values are compared to those for WT in Table 5. No AA was detected for the T68A and Q142A mutant enzymes.

Pyruvate Production. To determine whether pyruvate was produced when OAS was added to OASS, the reaction mixtures from the pre-steady state experiments with the T68A and Q142A mutant enzymes were assayed for the presence of pyruvate using NADH and lactate dehydrogenase. Significant pyruvate was present after a few hours.

Initial rates of pyruvate production, measured as the disappearance of NADH in the lactate dehydrogenase coupled assay, were obtained using 10 mM OAS, and rates were compared to that of the WT enzyme. The first-order rate constant for pyruvate production was obtained by dividing the initial rate by enzyme concentration. First-order rate constants for WT, T68A, and Q142A at pH 6.5 were 0.002, 0.007, and 0.3 s^{-1}, respectively.

DISCUSSION

Structural Analysis and Rationale for This Work. The structure of OASS-A has been determined to 2.2 Å resolution (*10*). The sulfhydrylase consists of two identical subunits, and each subunit has one active site, which is located deep in the protein, at the interface between the N- and C-terminal domains. The PLP cofactor in the active site cleft is in Schiff base linkage with the ε-amino group of K41, with its 5′-phosphate anchored by eight hydrogen bonds contributed by main chain and side chain functional groups in the glycine and threonine loop (176-GTGT-180). A total of eight hydrogen bonds anchor the PLP 5′-phosphate group, six from the residues in the loop and two from water molecules. The 5′-phosphate of the cofactor is dianionic as suggested by ^{31}P NMR spectra (*15*, *18*, *20*).

A superposition of the structures of the resting form (open form) and that of K41A, which exists as an ESB with methionine (closed form), an analogue of OAS, is shown in Figure 1. In the open form, the ε-amino group of K41 is bound to C4′ of the cofactor PLP in a Schiff base linkage. L-Methionine exists as an ESB in the K41A mutant enzyme, in a closed conformation (*9*, *11*). The active site closes to properly position active site functional groups for catalysis and exclude solvent. S69 in the substrate-binding loop moves 7 Å compared to its position in the open form and forms the two new hydrogen bonds, one with the α-carboxylate of the substrate and another with O3′ of the cofactor. In addition, the PLP tilts by 13° as the active site closes and the ESB is formed with the substrate. The closure of the active site is induced by the interaction between the substrate-binding loop and the α-carboxylate of the substrate, which leads to a reduction in the twist of the central β-sheet of the N-terminal domain. The conformational changes result in the formation of new hydrogen bonds and hydrophobic interactions between the N- and C-terminal domains. The microenvironment generated by these structural rearrangements stabilizes and orients the external aldimine for the elimination reaction and protects the highly reactive AA.

In the closed structure of the methionine ESB, the cofactor's O3′ atom is within hydrogen bonding distance of the amide nitrogen of N71 and the Schiff base nitrogen. Residues of the substrate-binding loop (T68, S69, and N71) in addition to Q142 bind the substrate α-carboxylate group in the ESB and subsequent intermediates along the reaction pathway. The relationship between the active site and the cofactor PLP is shown in Figure 1. The residues of the substrate binding loop (T68, S69, and N71) and Q142 are highly conserved from bacteria to plants (Figure 2). Data suggest the importance of the substrate binding loop and Q142 in the reaction mechanism.

Spectral and Kinetic Studies of Site-Directed Mutant Enzymes. The T68A and Q142A mutant enzymes exhibit only slight changes in their UV−visible spectra in the absence and presence of serine and cysteine, and the AA intermediate is not observed upon addition of OAS. The S69A and N71A mutant enzymes exhibit substantial changes in their UV−visible spectra in the presence of serine and cysteine, similar to WT, and a typical spectrum for the AA intermediate. Below, each of the mutant enzymes is discussed in terms of spectral and kinetic data obtained.

T68A Mutant Enzyme. The ISB of the T68A mutant enzyme is very similar to that of WT, as suggested by the UV−visible, fluorescence, near UV−visible CD, and ^{31}P NMR spectra. The serine and lanthionine ESBs exhibit only a slight increase in

the absorbance of the ketoenamine and enolimine tautomers, and only a slight red shift in the absorbance of the visible maximum. The presence of the ESBs is corroborated by an increase in the intrinsic tryptophan fluorescence at 337 nm, and an increase in ellipticity of the serine ESB at 414 nm compared to that of the ISB. However, no change in the 500 nm fluorescence is observed upon addition of serine or cysteine. Thus, either the position of the PLP relative to W50 does not change, or the lifetime of the excited state decreases in the T68A mutant enzyme. Addition of OAS gives no AA absorbance at 330 or 470 nm, no decrease in fluorescence at 500 nm, or a change in the near UV−visible CD spectrum compared to that of the ISB. The ^{31}P NMR spectra of the ISB and ESBs give identical chemical shifts and line widths, consistent with a lack of change in the environment around the 5′-phosphate of PLP. No formation of the AA was detected by stopped flow kinetic studies of the T68A mutant enzyme.

The AA is unstable in WT OASS at pH >6.5. The AA can be displaced by K41 to regenerate the ISB and free AA. The AA can tautomerize to iminopyruvate, which will be hydrolyzed to pyruvate and ammonia. Pyruvate is produced by the T68A mutant enzyme, which indicates the AA can be formed, but decomposes faster than it is formed. The rate of production of pyruvate is 3 times faster than that of WT. It is unlikely that this modest decrease in the stability of the AA accounts for its lack of buildup. As a result, the conversion of the ESB to the AA must also be slower. This proposal will be tested in future studies.

The strongest hydrogen bond (2.76 Å) to the α-carboxylate of the methionine ESB in the closed form of the enzyme is donated by the β-hydroxyl of T68 (Figure 1). Mutation of T68 to A generates an enzyme that appears to have either an open active site over the reaction time course or a more rapid conformational change to open and close the active site. The lack of buildup of the AA intermediate suggests the site is more open and consistent with the more rapid decomposition of the AA compared to WT and is much less stable, in agreement with the proposed role of T68 as part of the substrate-binding loop in triggering the conformational change to close the active site as the ESB is formed.

Q142A Mutant Enzyme. The UV−visible spectra of the Q142A mutant enzyme are qualitatively similar to those of T68A. The same slight red shift in the maximum of the visible band at 414 nm is observed for the serine and lanthionine ESBs, and the AA intermediate does not build up. Long wavelength fluorescence (500 nm) is observed but is lower than that of WT, and addition of serine or cysteine results in the enhancement of the 500 nm fluorescence, but not as much as WT. Thus, there is a change in the position of PLP relative to W50, but not to the same extent as WT. Data are in agreement with the formation of ESBs that are similar to those of WT. This can also be seen in the CD spectra, with increases in the ellipticity of the serine and lanthionine ESBs. Enhancement of long wavelength fluorescence and the intensity of the CD signal indicate the largest change is observed for the lanthionine ESB. The ^{31}P NMR chemical shift of the Q142A ISB and ESBs is the same as that of the WT. However, the line width of the ESBs is slightly broader than that of the ISB, but not as broad as those of WT. The substantial line broadening in the case of the WT enzyme can be interpreted in terms of relatively slow exchange between two conformers that represent the ketoenamine and enolimine tautomers of the ESB. The narrower line widths found for the Q142A mutant enzyme indicate a more rapid exchange rate, suggesting a more flexible site. The AA was not detected by stopped flow kinetic studies of the Q142A mutant enzyme. However, pyruvate is produced 150 times faster than WT, consistent with a much less stable AA that decomposes faster than it is formed.

Q142 is positioned above the PLP as one looks into the entrance to the active site and donates a hydrogen bond to the α-carboxylate of the ESB (2.83 Å) (Figure 1). As a result, Q142 aids in positioning the α-carboxylate, and thus the ESB, and shielding the AA intermediate to be formed from the ESB. Data are consistent with the proposed role of Q142. The loss of interaction of Q142 in the mutant enzyme may be expected to generate a less stable AA and affect the catalytic steps, consistent with the data.

S69A Mutant Enzyme. The UV−visible spectrum of the S69A mutant enzyme is qualitatively similar to that of the WT enzyme. Addition of OAS results in an AA spectrum identical to that of WT, indicative of the enzyme's ability to catalyze the first half-reaction. Formation of the AA is corroborated by the loss of long wavelength fluorescence, and the negative Cotton effect in the near UV−visible CD spectrum. In addition, pre-steady state kinetic data (Table 5) indicate the rate of the first half-reaction has decreased, but by a factor of only 9, and the dissociation constant for the OAS ESB has decreased by a factor of 4, giving a slight decrease (2-fold) in the second-order rate constant (k_{max}/K_{ESB}).

The serine ESB exhibits a spectrum that differs from that of WT. An increase in the absorbance of the ketoenamine tautomer is observed, but at 412 nm. There is no observable shift in the λ_{max}, and no significant increase in the absorbance at 330 nm reflecting the enolimine tautomer. Fluorescence spectra exhibit a significant increase in the emission at 337 nm, with very little change in emission at 500 nm, and there is no change in the near UV−visible CD spectrum. Thus, the active site environment of the serine ESB appears to be more hydrophilic than that of the WT and may suggest either a more open site or a more rapid opening and closing of the site. The fluorescence and CD data are consistent and suggest either a difference in the relative orientation of the PLP cofactor with respect to W50 or a decrease in the lifetime of the excited state.

The lanthionine ESB differs even more compared to the WT. The UV−visible spectrum exhibits only an increase in the absorbance below 330 nm, which reflects the thiolate of cysteine.[3] However, the 500 nm fluorescence increases slightly compared to that of the ISB; there is no significant change in the near UV−visible CD spectrum.

The ^{31}P NMR spectrum of the ISB is identical to that of WT in terms of the chemical shift and line width, consistent with little change in the resting, ISB, form of the enzyme. In the case of the ESBs, however, the chemical shift remains the same as that of the ISB, suggesting the environment around the 5′-phosphate does not change in all cases. The line widths are increased for the ESBs, but not as much as for WT, suggesting the rate of interconversion of the ketoenamine and enolimine tautomers is more rapid in the S69 mutant enzyme.

S69 changes its position by ~7 Å as the substrate-binding loop moves to interact with the α-carboxylate of the ESB. A new hydrogen bond [2.88 Å (Figure 1)] is formed between the carboxylate and the amide nitrogen on S69. Elimination of this interaction would be expected to affect the closing of the active site, and one might expect the transition from open to closed to be more rapid, consistent with the data.

N71A Mutant Enzyme. The N71A mutant enzyme behaves much more like the WT enzyme. The UV−visible spectrum of the

ISB is qualitatively identical to that of WT, as is that of the AA intermediate. Fluorescence emission and near UV−visible CD spectra of the ISB are also very similar to that of WT; a ratio of ~8 for emission at 337 nm to that at 500 nm is obtained compared to a ratio of 9 for WT, and the ellipticity at 412 nm is ~5 and ~6 mdeg for N71A and WT, respectively. The absorbance at 470 nm for the AA is the same as that of WT, but a slight increase in the absorbance at 330 nm is observed for N71A. The fluorescence spectra are also very similar, with a slight increase in the emission at 337 nm, and a loss of long wavelength fluorescence at 500 nm. However, a new band is observed at 550 nm, attributed to formation of the ketoenamine from the enolimine tautomer of the AA by proton transfer in the excited state. This mechanism was originally proposed to explain the ketoenamine fluorescence emission at 500 nm upon Trp excitation at 298 nm (*16*). These authors showed that the AA is weakly fluorescent. The CD spectrum of the AA exhibits a typical negative Cotton effect at 470 nm with approximately the same intensity as WT.

There are some differences in the spectra of the ESBs of serine and lanthionine. There was no red shift observed for the serine ESB, and the absorbance increased at 412 nm with no increase at 330 nm; that for the lanthionine ESB exhibited a red shift to 424 nm, with a shoulder at around 500 nm. A substantial increase in the long wavelength fluorescence was observed for both ESBs with the band for the serine ESB identical to that of WT, while that for the lanthionine ESB was slightly lower. Near UV−visible CD data corroborate the fluorescence data with greater intensity for the ESBs versus that found for WT. The ellipticity of the lanthionine ESB is almost twice that of WT. Taken together, these data indicate the ketoenamine tautomer of the ESB is stabilized in a manner consistent with a more hydrophilic site for N71A compared to WT.

As for all of the mutant enzymes, the ^{31}P NMR spectrum of the ISB is identical to that of WT in terms of the chemical shift and line width. In the case of the ESBs, however, the chemical shift remains the same as that of the ISB, suggesting the environment around the 5′-phosphate does not change. The line widths are increased for the ESBs, not as much as for WT but more than for the S69A mutant enzyme, suggesting the rate of interconversion of the ketoenamine and enolimine tautomers is more rapid in the S69A mutant enzyme.

The position of N71 in the substrate-binding loop exhibits the smallest change in position as the site closes on the ESB. Two hydrogen bonds are provided by N71, one from the side chain amide nitrogen to O3′ of the cofactor and another from the backbone NH group to the α-carboxylate of the ESB. Both hydrogen bonds are ~3 Å in length, suggesting the contribution to binding energy, and thus closing the site, is perhaps smaller for this residue than for S69. However, the effect on pre-steady state kinetics is greater for N71A than S69A, with a 1 order of magnitude decrease in k_{max} and a 2 order of magnitude decrease in k_{max}/K_{ESB}.

Investigations of other PLP-dependent enzymes have made use of mutations of loop or active site residues, detecting effects on the equilibrium distribution of catalytic intermediates as well as the equilibrium between open and closed states of the active site. Dunn and co-workers have conducted studies of tryptophan synthase (TS), while Kirsch and co-workers have conducted studies of aspartate aminotransferase (AAT). In TS, residues β-D305 and β-R141 are critical in stabilizing alternative catalytic intermediates as well as open and closed conformations via the formation of a salt bridge (*27*, *28*). In the internal Schiff base enzyme form, β-D305 does not interact with any other active site residue, while it forms a hydrogen bond with β-R141 in the ESB, stabilizing a partially open conformation. When the aminoacrylate Schiff base (AA) is formed in the active site, β-D305 interacts with β-R141 forming a salt bridge. Thus, it is not surprising that mutation of either D305 or R141 affects the equilibrium distribution between the ESB and AA as well as the open−closed equilibrium. The effect of mutations β-Q114N and β-T110V in TS was also investigated. Both amino acids are localized in the substrate recognition loop (β-110−115) and interact with the substrate α-carboxylate (*29*); Q114 is reminiscent of Q142 in OASS. In TS, Q114 was mutated to N. The shortening of the side chain was enough to strongly influence the enzyme reaction specificity, opening the way to the attack of AA. Mutation of Q142 to A in OASS-A also creates space that may favor an open active site conformation.

In AAT, the R292D mutation, in the so-called HEX enzyme (*30*), led to an increase in the flexibility of a small domain, which eliminated interaction with dicarboxylic acid substrates. In other PLP-dependent enzymes, including serine hydroxymethyltransferase (*31*), tyrosine phenol lyase (*32*), and cystathionine β-synthase (*33*), mutations of active site residues were exploited in investigating the role of specific amino acids in the stabilization of catalytic intermediates and, possibly, associated conformations.

Conclusions. Mutation of residues in the substrate-binding loop and Q142 has somewhat varied effects, but there are a number of generalizations that can be made. ^{31}P NMR spectra suggest the environment around the 5′-phosphate does not change significantly for any of the mutant enzymes, in a manner independent of the intermediate generated. However, the site appears to be more hydrophilic given that the ESBs exhibit smaller amounts of the enolimine tautomer. It appears that all of the tested mutations affect the opening and closing of the active site, but to different extents.

The T68A and Q142A mutant enzymes show no accumulation of the AA using either spectral probes or pre-steady state kinetic studies, suggesting both residues stabilize the ESB, the AA, or both. With respect to WT, pyruvate production is slightly greater for T68A, but much greater for Q142A. T68 donates a hydrogen bond to one of the carboxylate oxygens of the methionine ESB and is likely responsible for the proper orientation of the ESB to generate the AA and stabilization of the AA. Q142A, on the other hand, which also donates a hydrogen bond to one of the carboxylate oxygens of the methionine ESB, is involved in stabilizing the AA.

The S69A and N71A mutant enzymes exhibit formation of the AA, but k_{max}, the rate constant for formation of the AA from the ESB, is decreased by 1 order of magnitude compared to the WT rates for both enzymes. The second-order rate constant (k_{max}/K_{ESB}) is similar to that of WT for S69A but is decreased by 2 orders of magnitude for N71A. Of interest, N71 donates a hydrogen to O3′ of the cofactor, and another to the other oxygen of the methionine ESB, which may also affect the orientation of the ESB.

Overall, data demonstrate how reactivity, at the level of covalent PLP-bound intermediates, is derived in the *O*-acetylserine sulfhydrylase reaction. Interaction of intermediates with the substrate-binding loop and Q142, which shields the ESB and AA from solvent, allows active site closure to generate an active, properly aligned Michaelis complex and, subsequently, chemistry to occur.

SUPPORTING INFORMATION AVAILABLE

Figures showing the UV−visible, fluorescence, and CD spectra in the absence and presence of serine, cysteine, and OAS. This material is available free of charge via the Internet at http://pubs.acs.org.

REFERENCES

1. Kredich, N. M., and Tomkins, G. M. (1966) The Enzymatic Synthesis of L-Cysteine in *Escherichia coli* and *Salmonella typhimurium*. *J. Biol. Chem. 241*, 4955–4965.
2. Mino, K., and Ishikawa, K. (2003) Characterization of a Novel Thermostable *O*-Acetylserine Sulfhydrylase from *Aeropyrum pernix* K1. *J. Bacteriol. 185*, 2277–2284.
3. Tai, C.-H., Nalabolu, S. R., Jacobson, T. M., Minter, D. E., and Cook, P. F. (1993) Kinetic Mechanisms of the A and B Isozymes of *O*-Acetylserine Sulfhydrylase from *Salmonella typhimurium* LT-2 Using the Natural and Alternative Reactants. *Biochemistry 32*, 6433–6442.
4. Hwang, C.-C., Woehl, E. U., Dunn, M. F., and Cook, P. F. (1996) Kinetic Isotope Effects as a Probe of the β-Elimination Reaction Catalyzed by *O*-Acetylserine Sulfhydrylase. *Biochemistry 35*, 6358–6365.
5. Cook, P. F., and Wedding, R. T. (1976) A Reaction Mechanism from Steady State Kinetic Studies for *O*-Acetylserine Sulfhydrylase from *Salmonella typhimurium*. *J. Biol. Chem. 251*, 2023–2029.
6. Woehl, E., Dunn, M. F., Tai, C.-H., and Cook, P. F. (1996) Formation of the α-Aminoacrylate Intermediate Limits the Overall Reaction Catalyzed by *O*-Acetylserine Sulfhydrylase. *Biochemistry 35*, 4776–4783.
7. Rabeh, W. M., Alguindigue, S. S., and Cook, P. F. (2005) Mechanism of the Addition Half of the *O*-Acetylserine Sulfhydrylase-A Reaction. *Biochemistry 44*, 5541–5550.
8. Tai, C.-H., Nalabolu, S. R., Jacobson, T. M., Simmons, J. W., III, and Cook, P. F. (1995) Acid-base Chemical Mechanism of *O*-Acetylserine Sulfhydrylases-A and -B from pH Studies. *Biochemistry 34*, 12311–12322.
9. Rege, V. D., Kredich, N. M., Tai, C.-H., Karsten, W. E., Schnackerz, K. D., and Cook, P. F. (1996) A Change in the Internal Aldimine Lysine (K42) in *O*-Acetylserine Sulfhydrylase to Alanine Indicates Its Importance in Transimination and as a General Base Catalyst. *Biochemistry 35*, 13485–13493.
10. Burkhard, P., Tai, C.-H., Ristroph, C. M., Cook, P. F., and Jansonius, J. N. (1999) Ligand Binding Induces a Large Conformational Change in *O*-Acetylserine Sulfhydrylase from *Salmonella typhimurium*. *J. Mol. Biol. 291*, 941–953.
11. Burkhard, P., Rao., G. S., Hohenester, E., Schnackerz, K. D., Cook, P. F., and Jansonius, J. N. (1998) Three-dimensional Structure of *O*-Acetylserine Sulfhydrylase from *Salmonella typhimurium*. *J. Mol. Biol. 283*, 121–133.
12. Rabeh, W. M., and Cook, P. F. (2004) Structure and Mechanism of *O*-Acetylserine Sulfhydrylase. *J. Biol. Chem. 279*, 26803–26806.
13. Burkhard, P., Tai, C.-H., Jansonius, J. N., and Cook, P. F. (2000) Identification of an Allosteric Anion-binding Site on *O*-Acetylserine Sulfhydrylase: Structure of the Enzyme with Chloride Bound. *J. Mol. Biol. 303*, 279–286.
14. Strambini, G., Cioni, P., and Cook, P. F. (1996) Tryptophan and Coenzyme Luminescence as a Probe of Conformation Along the *O*-Acetylserine Sulfhydrylase Reaction Pathway. *Biochemistry 35*, 8392–8400.
15. Schnackerz, K. D., Tai, C.-H., Simmons, J. W., III, Jacobson, T. M., Rao, G. S. J., and Cook, P. F. (1995) Identification and Characterization of the External Aldimine Intermediate of the *O*-Acetylserine Sulfhydrylase Reaction. *Biochemistry 34*, 12152–12160.
16. Benci, S., Vaccari, S., Mozzarelli, A., and Cook, P. F. (1997) Time-Resolved Fluorescence of *O*-Acetylserine Sulfhydrylase Catalytic Intermediates. *Biochemistry 36*, 15419–15427.
17. Rabeh, W., Alguindigue, S. S., and Cook, P. F. (2005) Mechanism of the Addition Half of the *O*-Acetylserine Sulfhydrylase-A Reaction. *Biochemistry 44*, 5541–5550.
18. Cook, P. F., Hara, S., Nalabolu, S., and Schnackerz, K. D. (1992) pH Dependence of the Absorbance and ^{31}P NMR Spectra of *O*-Acetylserine Sulfhydrylase in the Absence and Presence of *O*-Acetyl-L-Serine. *Biochemistry 31*, 2298–2303.
19. McClure, G. D., and Cook, P. F. (1994) Product Binding to the α-Carboxyl Subsite Results in a Conformational Change at the Active Site of *O*-Acetylserine Sulfhydrylase-A: Evidence from Fluorescence Spectroscopy. *Biochemistry 33*, 1674–1683.
20. Schnackerz, K. D., and Cook, P. F. (1995) Resolution of the Pyridoxal 5′-Phosphate from *O*-Acetylserine Sulfhydrylase and Reconstitution with the Native Cofactor and Analogs. *Arch. Biochem. Biophys. 324*, 71–77.
21. Flint, D. H., Tuminello, J. F., and Miller, T. J. (1996) Studies on the Synthesis of the Fe-S Cluster of Dihydroxy-acid Dehydratase in *Escherichia coli* Crude Extract. Isolation of *O*-Acetylserine Sulfhydrylases A and B and β-Cystathionase Based on their Ability to Mobilize Sulfur from Cysteine and to Participate in Fe-S Cluster Synthesis. *J. Biol. Chem. 271*, 16053–16067.
22. Benci, S., Bettati, S., Vaccari, S., Schianchi, G., Cook, P. F., and Mozzarelli, A. (1999) *O*-Acetylserine Sulfhydrylase Probed by Static and Time-Resolved Tryptophan Fluorescence During Catalysis. *J. Photochem. Photobiol. 48*, 17–26.
23. Campanini, B., Raboni, S., Vaccari, S., Zhang, L., Cook, P. F., Hazlett, T. L., Mozzarelli, A., and Bettati, S. (2003) Surface-Exposed Tryptophan residues Are Essential for *O*-Acetylserine Sulfhydrylase Structure, Function, and Stability. *J. Biol. Chem. 278*, 37511–37519.
24. Cantor, C. R., and Shimmel, P. R. (1980) Biophysical Chemistry: Part III: Techniques for the Study of Biological Structure and Function, W. H. Freeman, San Francisco.
25. Guan, R. (2009) Mechanisms of Serine Acetyltransferase and O-Acetylserine Sulfhydrylase. Ph.D. Dissertation, University of Oklahoma, Norman, OK.
26. Li, L., and Cook, P. F. (2006) The 2′-Phosphate of NADP Is Responsible for Proper Orientation of the Nicotinamide Ring in the Oxidative Decarboxylation Reaction Catalyzed by Sheep Liver 6-Phosphogluconate Dehydrogenase. *J. Biol. Chem. 281*, 36803–36810.
27. Ferrari, D., Yang, L. H., Miles, E. W., and Dunn, M. F. (2001) βD305A Mutant of Tryptophan Synthase Shows Strongly Perturbed Allosteric Regulation and Substrate Specificity. *Biochemistry 40*, 7421–7432.
28. Ferrari, D., Niks, D., Yang, L. H., Miles, E. W., and Dunn, M. F. (2003) Allosteric Communication in the Tryptophan Synthase Bienzyme Complex: Roles of the β-Subunit Aspartate 305/Arginine 141 Salt Bridge. *Biochemistry 42*, 7807–7818.
29. Blumenstein, L., Domratcheva, T., Niks, D., Ngo, H., Seidel, R., Dunn, M. F., and Schlichting, I. (2007) βQ114N and βT110V Mutations Reveal a Critically Important Role of the Substrate α-Carboxylate Site in the Reaction Specificity of Tryptophan Synthase. *Biochemistry 46*, 14100–14016.
30. Chow, M. A., McElroy, K. E., Corbett, K. D., Berger, J. M., and Kirsch, J. F. (2004) Narrowing Substrate Specificity in a Directly Evolved Enzyme: The A293D Mutant of Aspartate Aminotransferase. *Biochemistry 43*, 12780–12787.
31. Delle Fratte, S., Iurescia, S., Angelaccio, S., Bossa, F., and Schirch, V. (1994) The Function of Arginine 363 as the Carboxyl-binding Site in *Escherichia coli* Serine Hydroxymethyltransferase. *Eur. J. Biochem. 225*, 395–401.
32. Demidkina, T. V., Zakomirdina, L. N., Kulikova, V. V., Dementieva, I. S., Faleev, N. G., Ronda, L., Mozzarelli, A., Gollnick, P. D., and Phillips, R. S. (2003) Role of Aspartate-133 and Histidine-458 in the Mechanism of Tryptophan Indole-lyase from *Proteus vulgaris*. *Biochemistry 42*, 11161–11169.
33. Aitken, S. M., and Kirsch, J. F. (2004) Role of Active-site Residues Thr81, Ser82, Thr85, Gln157, and Tyr158 in Yeast Cystathionine β-Synthase Catalysis and Reaction Specificity. *Biochemistry 43*, 1963–1971.
34. Demchenko, A. P. (1986) Ultraviolet Spectroscopy of Proteins, p 21, Springer-Verlag, Berlin.
35. Gouet, P., Courcelle, E., Stuart, D. I., and Metoz, F. (1999) ESPript: Analysis of Multiple Sequence Alignments in PostScript. *Bioinformatics 15*, 305–308.